Some experiences at SOLEIL on the beam-induced heating of the vacuum components

Workshop on "Simulation of Power Dissipation and Heating from Wake Losses in Accelerator Structures"

30 January 2013, DIAMOND Light Source

R. Nagaoka, on behalf of the SOLEIL accelerator team

Abstract:

Numerical and experimental studies on wakefields, instabilities and beam-induced heating at SOLEIL are reviewed, including the ion instability encountered at 500 mA at SOLEIL, which is considered to arise from the beam-induced vacuum components heating.

Contents:

1. Flange

cf) R. Nagaoka, "Numerical evaluation of …", EPAC 2004, Lucerne

◊ A model having a slit of 0.4 mm long and 50 mm deep with no shielding was initially considered.

Calculated impedance exhibited strong trapped modes in all planes **at low frequencies** besides large BB impedance. As unacceptably low multibunch instability thresholds were found, a detailed study was launched

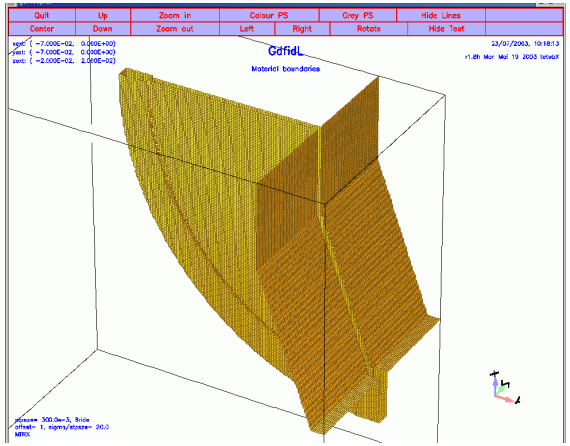

Flange with a slit of 0.4 mm long and 50 mm deep

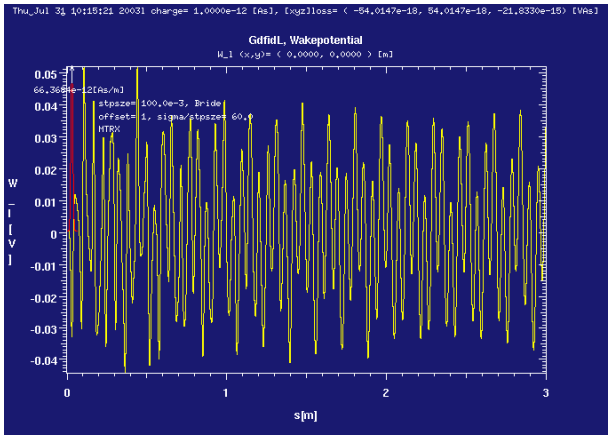

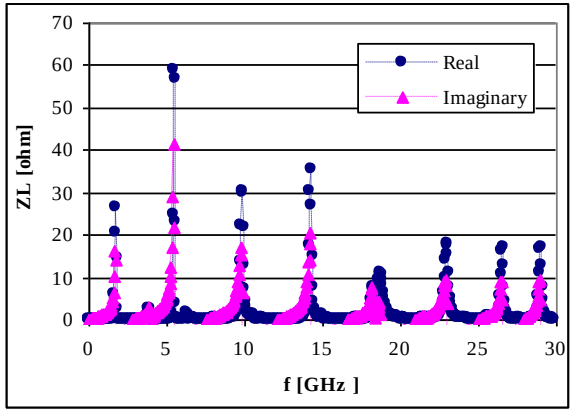

Calculated longitudinal wake (left) and impedance (right)

⇨ Dependence of the impact on the slit length, depth and *Q*-values was followed

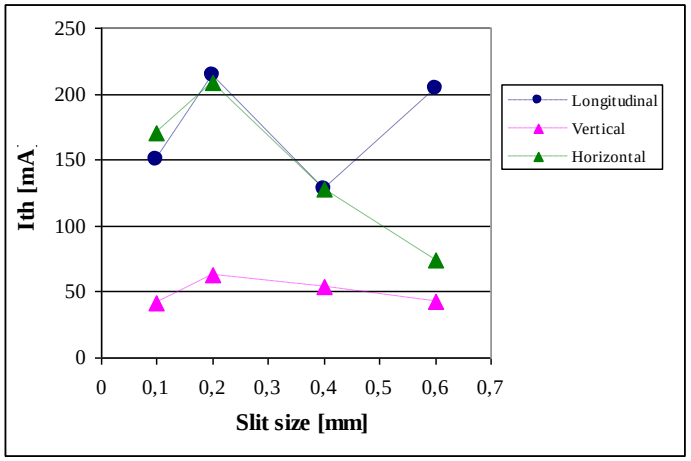

◊ Dependence on the slit size:

- Resonant frequencies depend little on the slit size
- Amplitudes grow with the slit size, but not rapidly

Coupled-bunch instability thresholds versus slit size (length)

◊ Dependence on the slit depth:

→ *Up to ~3 mm depth may be tolerated*

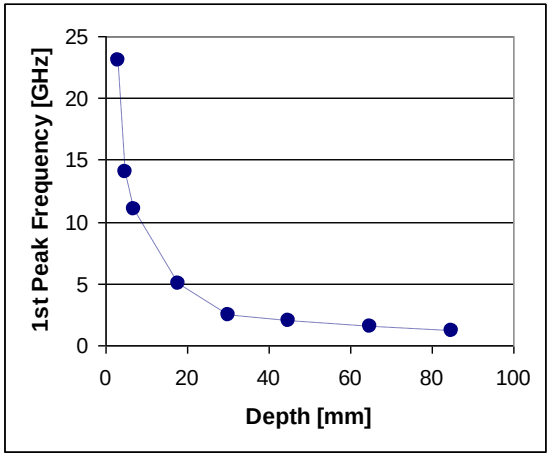

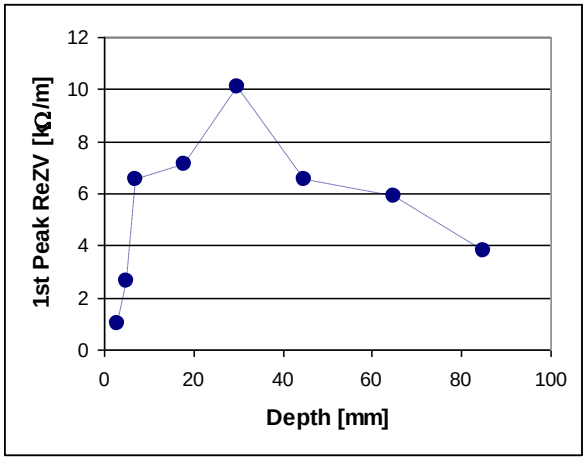

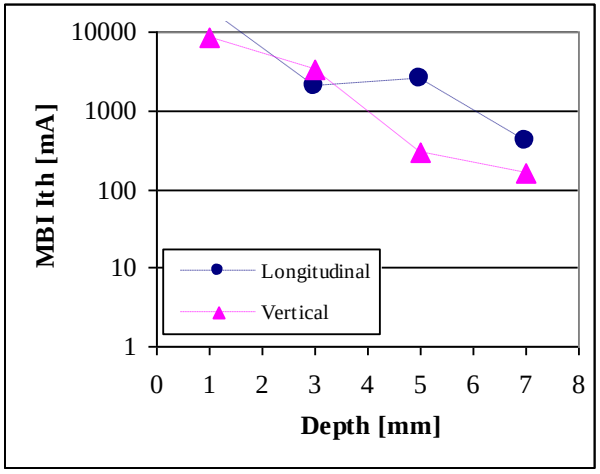

- Large dependence found. Variation is particularly pronounced at small depth

◊ Dependence on the *Q* values of resonant modes:

- Time domain calculations: *Q :* Indefinite → Convergence attained on *R*/*Q*
- Eigenvalue calculations with finite *Q* and identification of modes with the time domain
- Use of the found *R*/*Q* values in the instability calculations → No significant change on I_{th}

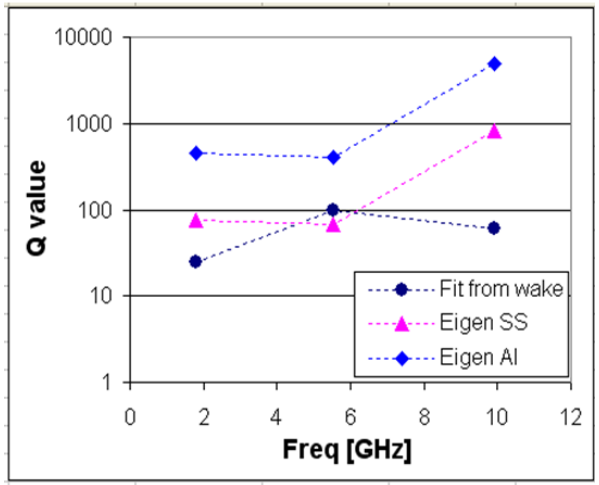

Slit = 0.4 mm			
File = Gap0.4VFx_EigenSTPSZE=300.00e-3			
	Q-values		
freq [GHz]	Fitted from Z	StainlessS	Aluminium
1,78	25	76,0	455,9
5,53	100	68,6	411,6
9,9	60	818,5	4910,8
Ith [mA]	**52**	**56**	

Dependence of instability threshold I_{th} on Q values

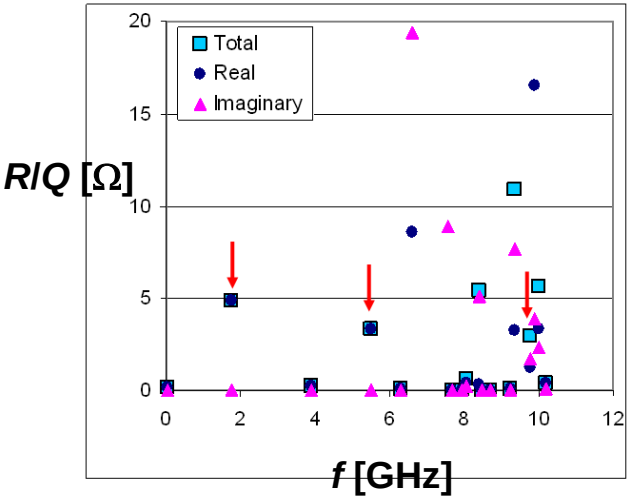

Slit = 0.4 mm

Identification of modes between time and frequency domain calculations

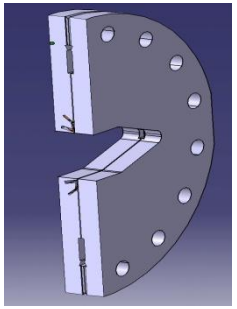

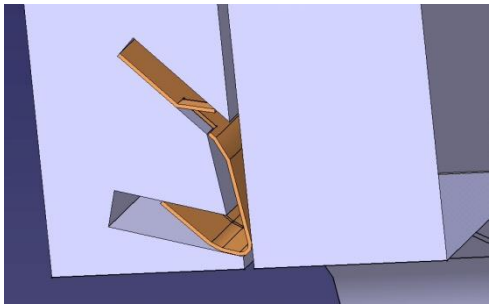

⇨ Introduction of a shielding foil drastically reduced the impedance

2. BPM

cf) R. Nagaoka et al., "Recent studies of …", EPAC 2006, Edinburgh

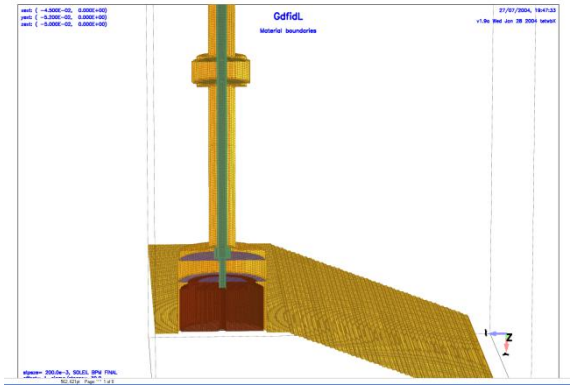

- Impedance of a SOLEIL BPM was studied with *GdfidL* by including the entire feedthrough structure under the waveguide boundary condition, minimising the reflection simultaneously

- Reduction of the button diameter was avoided as it lowers the button sensitivity ($\propto r^2$) . Instead the button thickness was sought to increase, finding that a change from 2 to 5 mm reduces the loss factor by as much as a factor of 2

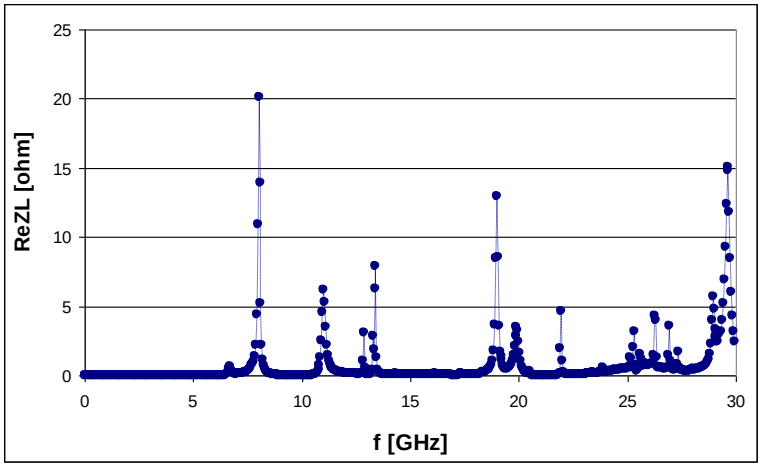

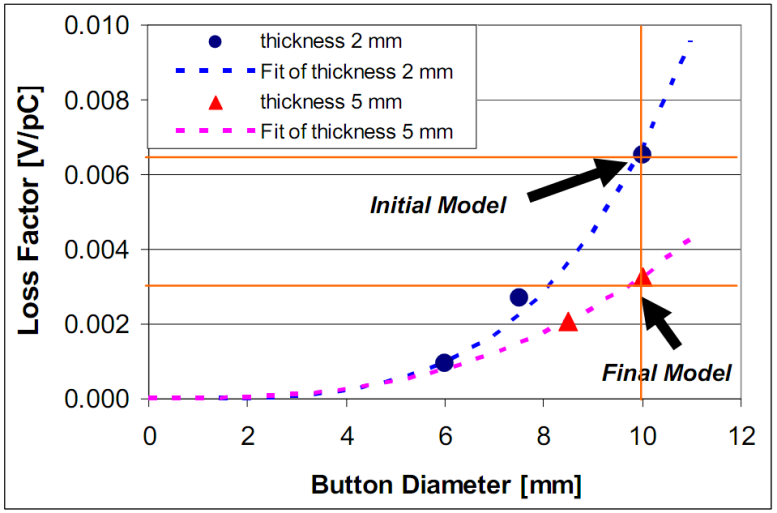

- Problem encountered is a mode strongly trapped between the button and the block around 8 GHz, which is expected to be *TE110*

- In view of the risk of spoiling the BPM accuracy due to dilation of the button, the heat that goes into the button was evaluated with the surface integral

$$\iint \frac{H_{//}^2}{2\kappa\delta}\, dF \quad [\mathrm{W}]$$

$H_{//}$: Tangential magnetic field
κ : Conductivity
δ : Skin depth at the resonant frequency

s [m]	t [sec]	Total structure metalpower [W*sec]	Button only metalpower [W*sec]	ratio
0,70	2,33E-09	1,79E-08	8,57E-09	2,09
0,71	2,37E-09	1,93E-07	9,60E-08	2,01
0,72	2,40E-09	1,38E-08	6,74E-09	2,05
0,73	2,44E-09	1,34E-07	6,81E-08	1,97

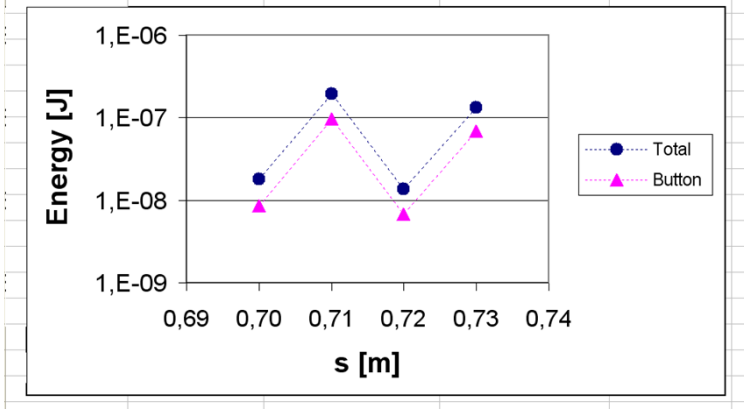

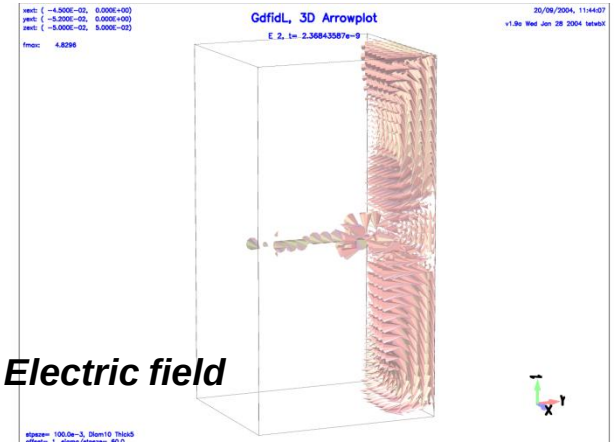

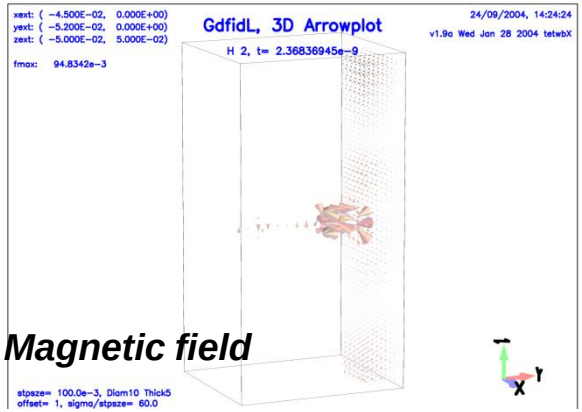

- By assuming in one case that the BPM block is superconducting, a half of the Joule loss was concluded to arise from the button, signifying the power on the button to be around 0.6 W at 500 mA

- Study was extended to include a coupled-bunch effect on the loss factor, which may increase the net beam power experienced by an electrode

$$k_{loss} = \frac{1}{\pi}\sum_{m=0}^{\infty}\int_{0}^{\infty} \mathrm{Re}\, Z_{//}(\omega)\cdot e^{-\sigma_\tau^2\omega^2}\cos(m\Delta T\omega)\, d\omega \qquad \Delta T : \text{RF period}$$

  - Effective damping time of the trapped mode estimated by equating the wall energy loss integrated over time to the single bunch energy loss, and then defined the resonant *Q*-value accordingly (→ roughly 3*ΔT found)

Material Block/ button	Q	k_{loss} ratio	P_{tot} [W]	P_{button} [W]	T_{button} [°C]	Curr. dep. [μm]
S.S/S.S	211	3.43	4.18	2.09	180	4.1
S.S/Gold	366	5.45	6.65	0.89	88	1.7
S.S/S.S	Low	1.00	1.22	0.61	68	1.2

Button displacement between 0 and 500 mA

- An enhanced power of 2.1 W/electrode against the original 0.6 W found, in the worst case when the trapped mode is in resonance with the RF
- Gold coating of the button would reduce from 2.1 to 0.9 W the power deposited on the button, but the idea was abandoned due to technical complications
- In reality, a certain number of BPMs show anomalous behaviour depending on beam current, beam filling and bunch length, and are being replaced with buttons made of molybdenum, which is a simple solution similar to the gold coating. Most of the power goes to the block

3. In-vacuum insertion device taper

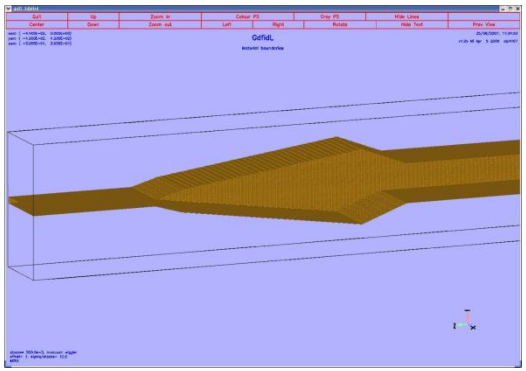

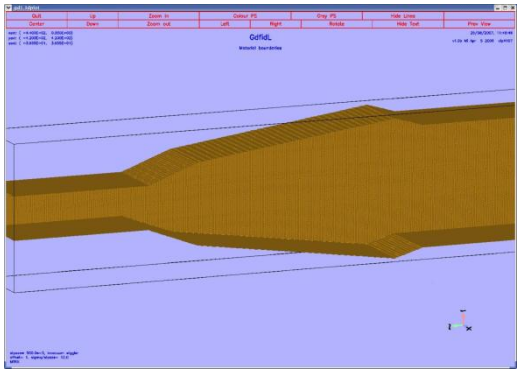

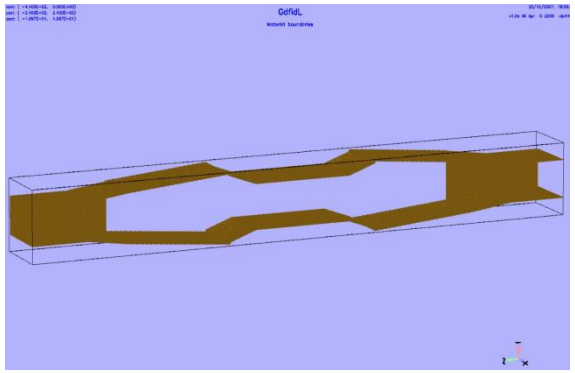

Initial taper model: (Left) Gap at 5.5 mm. (Right) Gap at 30 mm

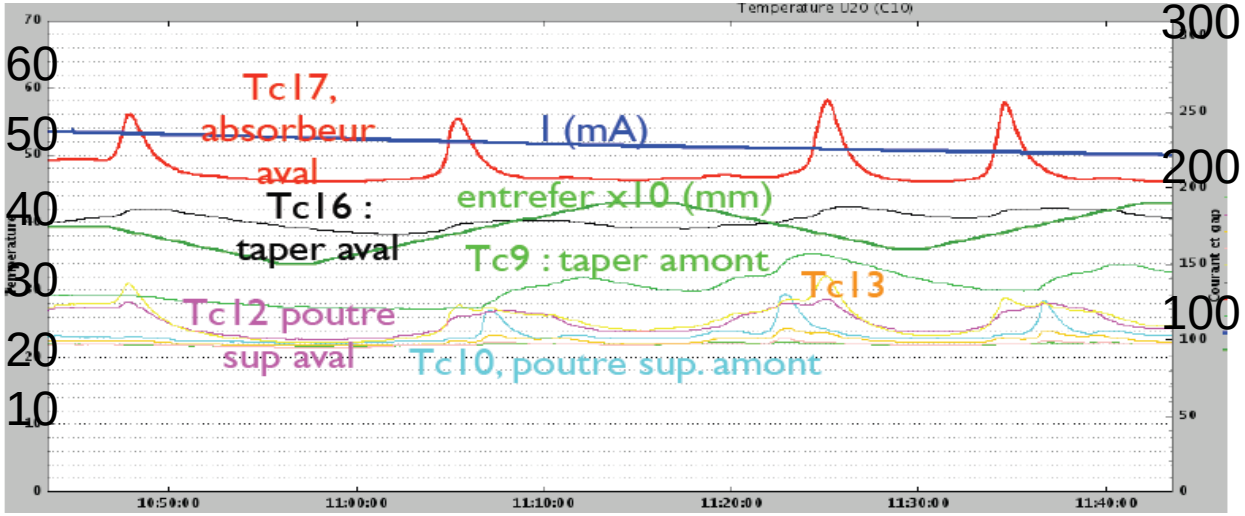

Observed heating of an in-vacuum insertion device (U20) with beam

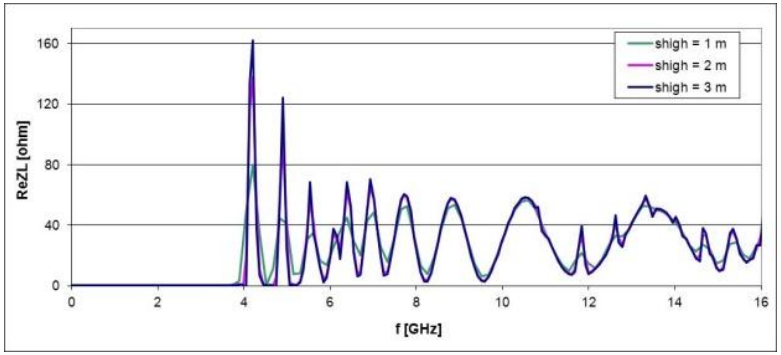

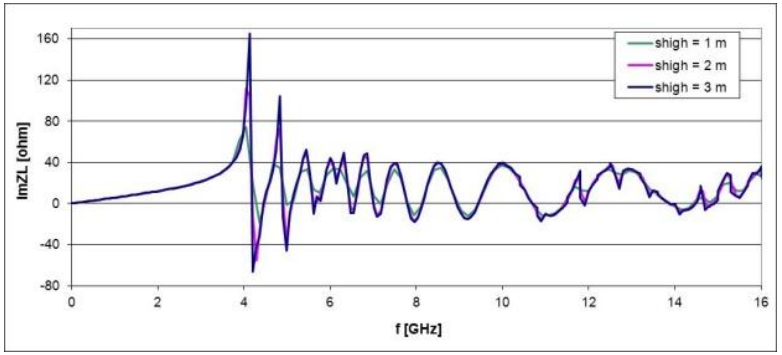

Real (left) and Imaginary (right) parts of the longitudinal impedance of the taper calculated at gap = 30 mm (open position), showing resonant behaviour from ~4 GHz upwards

⇨ The new taper designed and constructed avoided the cavity-like structure and better linearised the transition

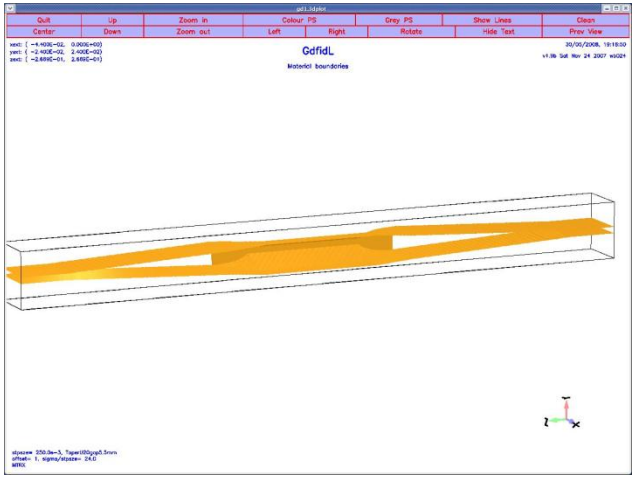

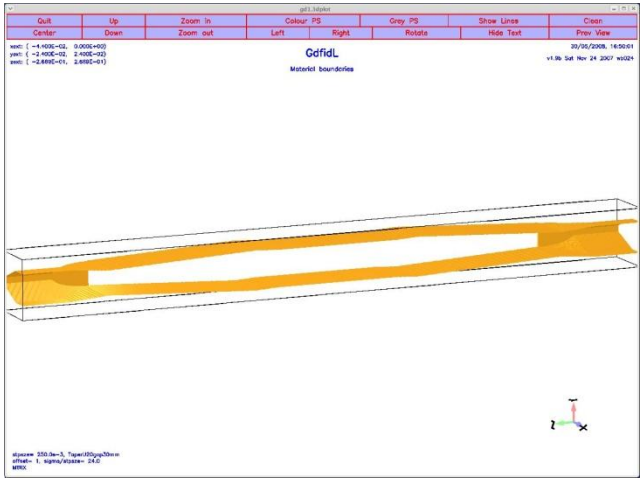

New taper model: (Left) Gap at 5.5 mm. (Right) Gap at 30 mm

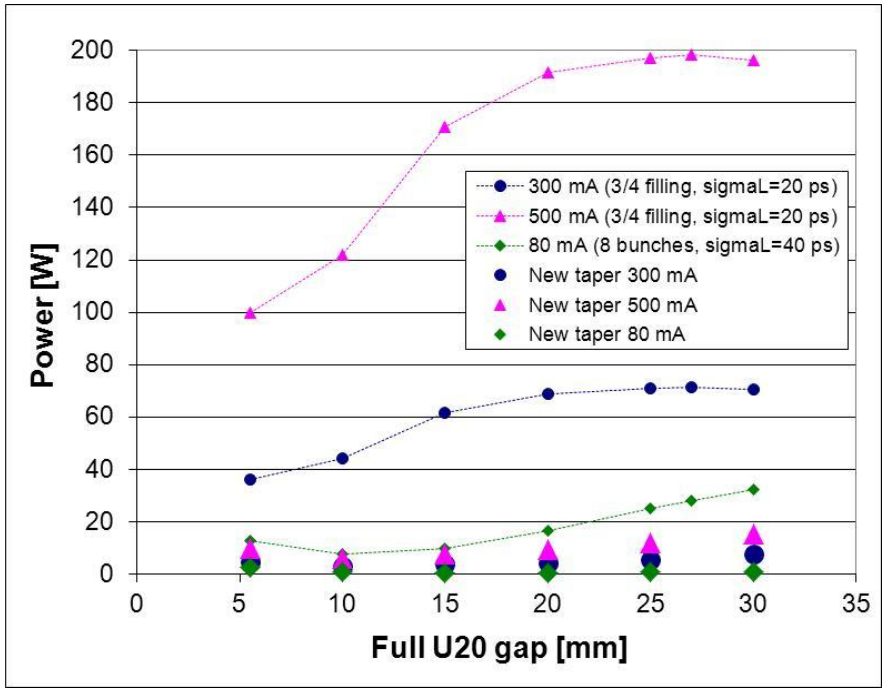

Comparison of evaluated beam-induced power between the old and the new taper models as a function of the gap in different filling modes

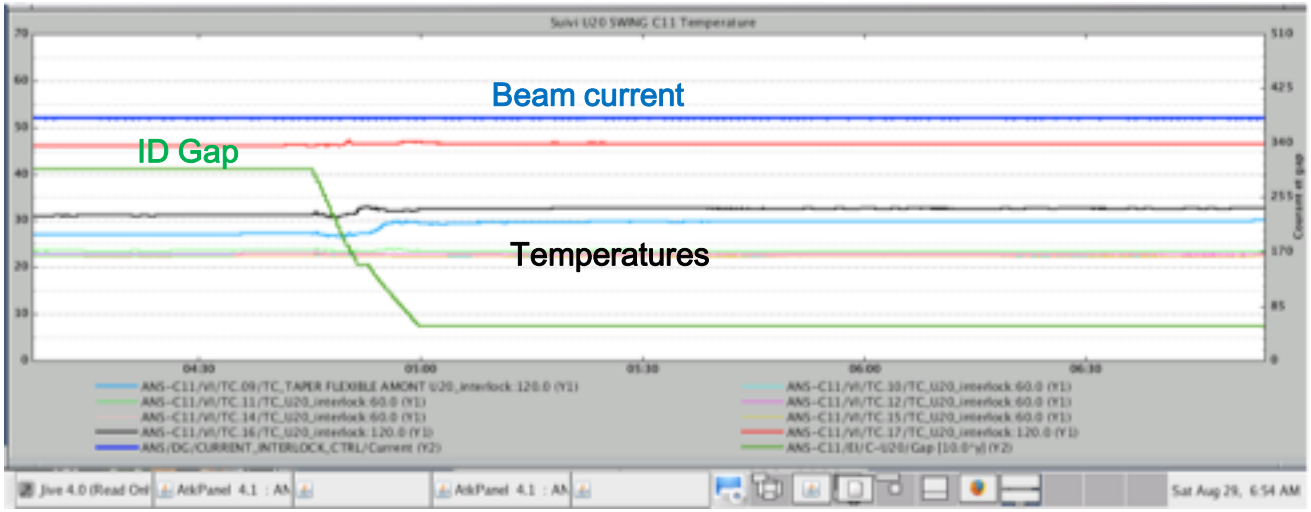

As expected, beam-induced heating could be greatly reduced with the new taper

4. Striplines

cf) R. Nagaoka et al., "Recent studies of …", EPAC 2006, Edinburgh
C. Mariette et al., "Excitation stripline for …", DIPAC 2007, Venice

◊ Up to now, three striplines have been designed and installed in the storage ring:

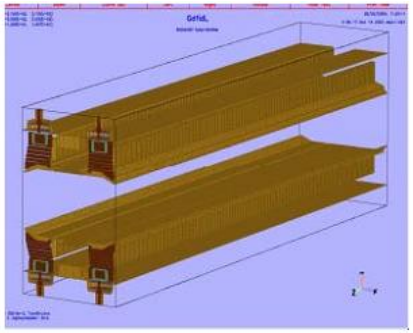

4-electrode and short-circuited on one end

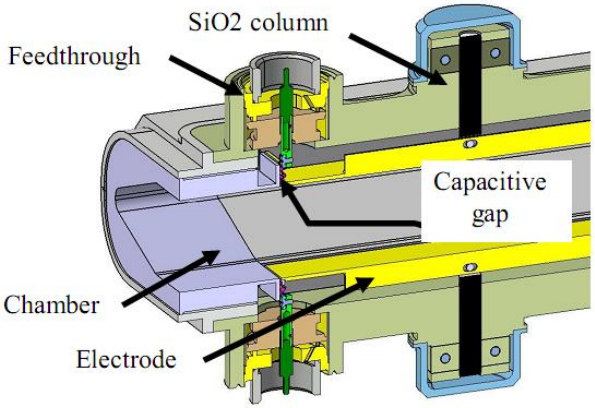

2-electrode, used for the vertical feedback

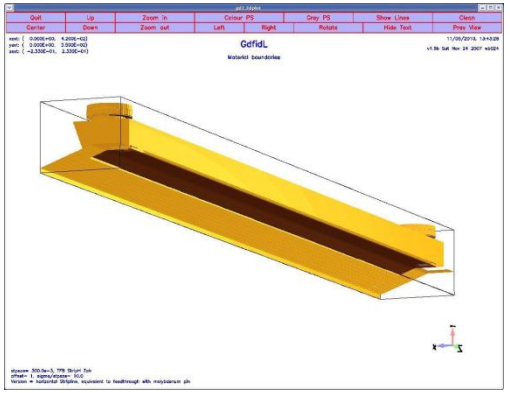

4-electrode, used for the horizontal feedback (1/4 structure shown)

- In all cases, the electrodes are smoothly embedded in the vacuum chamber with no transition in between
- A capacitive gap of 0.3 ~ 0.5 mm is introduced between the electrode and the chamber, which filters out high frequency components of beam power from propagating into the feedthrough. The loss factor is expected to be reduced in this way by a factor of 2

cf) J.-C. Denard et al., "Parasitic mode losses …", SLAC-PUB-3654, April 1985 (A)

◊ Three types of time-domain computations were made with *GdfidL*:

- Port excitation for the signal transmission optimisation in the feedthrough (as in the BPM)
- Port excitation for the evaluation of the shunt impedance (transverse kick efficiency)
- Wake potential computation

	Loss V/pC	$\mathrm{Re}(ZL)_{eff}$ Ω	$\mathrm{Im}(ZL/n)_{eff}$ mΩ
TFB stripline	0.075	5.30	1.62
Tune stripline	0.007	0.48	0.27
120 BPMs	0.360	28.80	13.2
V scraper	0.453	32.13	7.03

	$\mathrm{Re}(ZV)_{eff}$ at $\xi = 0.3$ kΩ/m	$\mathrm{Im}(ZV)_{eff}$ kΩ/m
TFB stripline	0.46	0.88
Tune stripline	0.02	0.03
120 BPMs	2.4	4.8
V scraper	2.8	4.88

Comparison of calculated longitudinal (upper) and vertical (lower) impedance of the vertical stripline (TFB stripline) and shorted stripline (Tune stripline) with BPMs and a vertical scraper

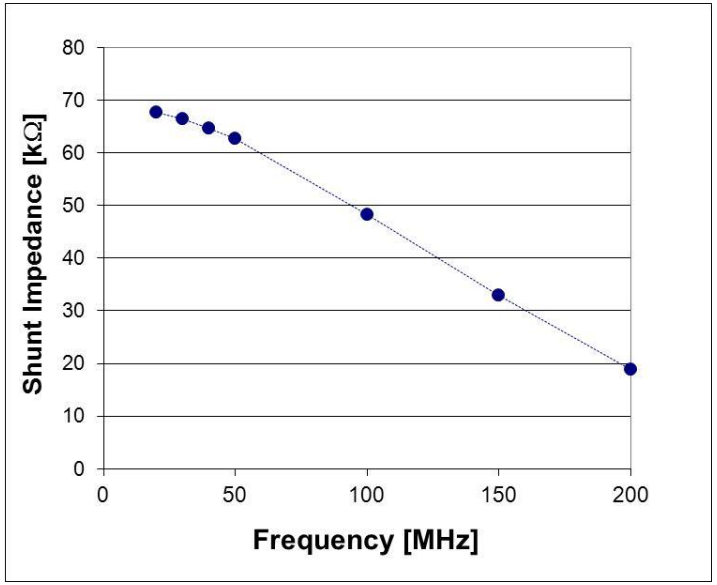

Transverse shunt impedance calculated for the vertical stripline

⇨ Striplines with high shunt impedance and low coupling impedance were constructed

5. Resistive-wall and ceramic chamber

◊ Resistive-wall

cf) R. Nagaoka, "Study of resistive-wall effects …", EPAC 2004, Lucerne
R. Nagaoka, "Numerical evaluation of …", EPAC 2004, Lucerne

C Name	s1 [m]	s2 [m]	a0 [mm]	b0 [mm]	d0 [mm]	rho [ohm*m]	shape	surface	dV/dy	r	keffs [m-2]	<betaH> [m]	<betaV> [m]
IDLD_S1	0.000	5.434	35.000	12.500	2.000	2.80e-08	elli	Coat	3.63e-02	1.00	4.18e-07	11.06	9.23
SIND_S1.1	5.434	5.864	35.000	12.500	2.000	2.80e-08	elli	Coat	3.63e-02	1.00	4.18e-07	13.25	11.99
BPM_S1.1	5.864	6.064	42.000	12.500	17.000	1.00e-06	elli	NoCo	2.17e-01	1.00	1.00e-06	13.55	12.38
SIND_S1.2	6.064	7.234	35.000	12.500	2.000	2.80e-08	elli	Coat	3.63e-02	1.00	4.18e-07	20.18	9.38
BPM_S1.2	7.234	7.434	42.000	12.500	17.000	1.00e-06	elli	NoCo	2.17e-01	1.00	1.00e-06	23.10	7.33
SIND_S1.3	7.434	8.948	35.000	12.500	2.000	2.80e-08	elli	Coat	3.63e-02	1.00	4.18e-07	9.79	11.85
SOUF_S1.1	8.948	9.089	42.000	12.500	17.000	1.00e-06	elli	NoCo	2.17e-01	1.00	1.00e-06	2.58	14.30
BEND_S1.1	9.089	10.677	35.000	12.500	2.000	1.00e-06	elli	NoCo	2.17e-01	1.00	1.00e-06	0.94	15.90
SIND_S1.4	10.677	11.147	35.000	12.500	2.000	2.80e-08	elli	Coat	3.63e-02	1.00	4.18e-07	3.17	16.55
BPM_S1.3	11.147	11.347	42.000	12.500	17.000	1.00e-06	elli	NoCo	2.17e-01	1.00	1.00e-06	6.22	13.35
SIND_S1.5	11.347	12.413	35.000	12.500	2.000	2.80e-08	elli	Coat	3.63e-02	1.00	4.18e-07	13.91	7.91
BPM_S1.4	12.413	12.613	42.000	12.500	17.000	1.00e-06	elli	NoCo	2.17e-01	1.00	1.00e-06	16.71	6.44
SIND_S1.6	12.613	13.679	35.000	12.500	2.000	2.80e-08	elli	Coat	3.63e-02	1.00	4.18e-07	14.48	7.55
BPM_S1.5	13.679	13.879	42.000	12.500	17.000	1.00e-06	elli	NoCo	2.17e-01	1.00	1.00e-06	7.05	12.49
SIND_S1.7	13.879	14.453	35.000	12.500	2.000	2.80e-08	elli	Coat	3.63e-02	1.00	4.18e-07	3.35	16.29
SOUF_S1.2	14.453	14.594	42.000	12.500	17.000	1.00e-06	elli	NoCo	2.17e-01	1.00	1.00e-06	1.45	17.03
BEND_S1.2	14.594	16.182	35.000	12.500	2.000	1.00e-06	elli	NoCo	2.17e-01	1.00	1.00e-06	1.08	15.60
SIND_S1.8	16.182	17.042	35.000	12.500	2.000	2.80e-08	elli	Coat	3.63e-02	1.00	4.18e-07	7.26	11.29
BPM_S1.6	17.042	17.242	42.000	12.500	17.000	1.00e-06	elli	NoCo	2.17e-01	1.00	1.00e-06	15.00	6.61
SIND_S1.9	17.242	18.412	35.000	12.500	2.000	2.80e-08	elli	Coat	3.63e-02	1.00	4.18e-07	13.67	6.70
BPM_S1.7	18.412	18.693	42.000	12.500	17.000	1.00e-06	elli	NoCo	2.17e-01	1.00	1.00e-06	7.06	8.58
SIND_S1.10	18.693	19.406	35.000	12.500	2.000	2.80e-08	elli	Coat	3.63e-02	1.00	4.18e-07	6.23	6.82
CVTP2U_S2	19.406	19.634	42.500	31.250	1.000	1.00e-06	elli	NoCo	1.00e-02	1.00	5.00e-08	5.55	5.32
CVTB2U_S2	19.634	19.892	50.000	50.000	1.000	1.00e-06	circ	NoCo	0.00e+00	1.00	0.00e+00	5.28	4.68
CVTP1U_S2	19.892	20.217	90.000	90.000	1.000	1.00e-06	circ	NoCo	0.00e+00	1.00	0.00e+00	4.97	3.98
CVTB1U_S2	20.217	20.570	130.000	130.000	1.000	1.00e-06	circ	Coat	0.00e+00	1.00	0.00e+00	4.65	3.28
SCCVU_S2	20.570	22.030	130.000	130.000	1.000	0.00e+00	circ	NoCo	0.00e+00	1.00	0.00e+00	4.17	2.17
SCCVD_S2	22.030	23.490	130.000	130.000	1.000	0.00e+00	circ	NoCo	0.00e+00	1.00	0.00e+00	4.17	2.17
CVTB1D_S2	23.490	23.843	130.000	130.000	1.000	1.00e-06	circ	Coat	0.00e+00	1.00	0.00e+00	4.65	3.28

Machine data file

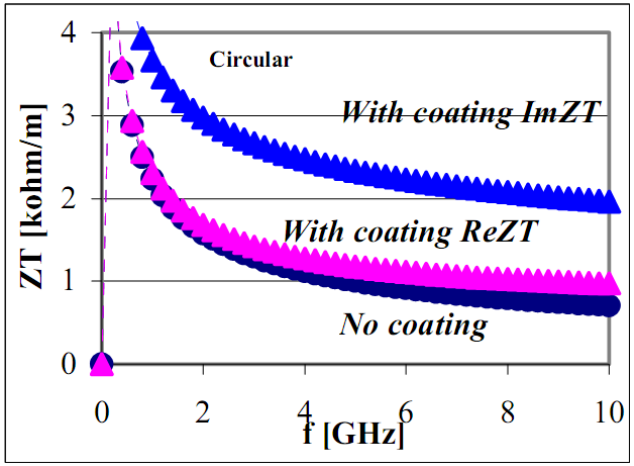

Transverse impedance with and without NEG coating

- A machine file was prepared containing all the basic information related to the RW (metallic coating, thickness, …) and the optics, for each chamber around the ring

- With 1 µm thickness NEG and the resistivity of 25×10^{-8} Ωm, of Vanadium (the constituent material with the lowest resistivity), the reactive part is nearly doubled, while the resistive part is roughly unchanged in the frequency range up to ~10 GHz

- Although distributed around the ring, the beam-induced power due to RW is estimated to represent more than 50% of the total

◊ Ceramic chamber

cf) R. Nagaoka et al., "Recent studies of …", EPAC 2006, Edinburgh, and in close collaboration with Pierre Lebasque at SOLEIL

- To evaluate the heating of titanium coated ceramic chambers used for kickers and shakers, their longitudinal impedance was studied analytically
- EM field matching with different metallic layers was extended to include dielectric materials in the MKSA unit, working with (*E*, *H*)

$$\frac{Z_{//}(\omega)}{L} = \frac{-i}{2\pi\varepsilon_0 cb}\left\{\left(\frac{a}{k}-\frac{k}{a}\right)\cdot\frac{\left[1+A\tanh(ad)\right]}{\left[A+\tanh(ad)\right]}-\frac{kb}{2}\right\}^{-1}$$

k=ω/c, a=[1-i·sgn(ω)]/d_s (d_s: skin depth)

d : titanium coating thickness

- Since the image current is proportional to E_z in the metal, its radial dependence was followed at as a function of frequency

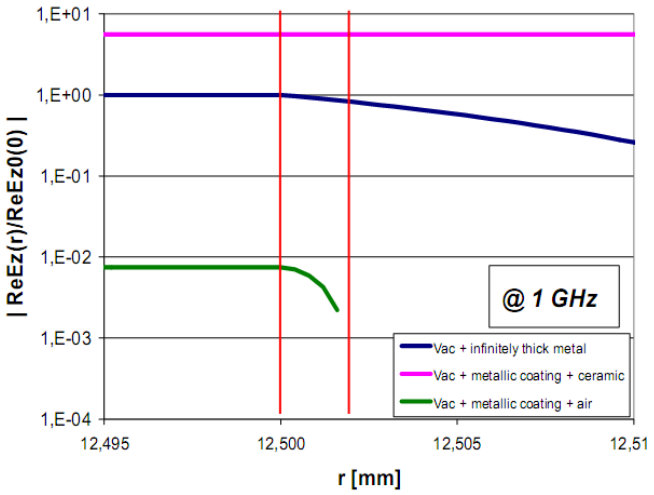

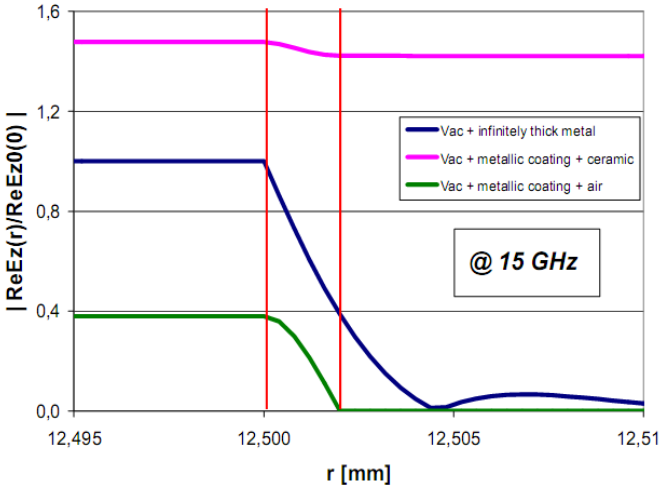

⇨

It is found that ceramic compresses the EM field in the coating

- Surface power density, which is more directly related to the temperature distribution along the perimeter, was also studied, using Piwinski's formulation on a flat chamber, solving analytically EM fields in the transverse plane

$$P_s(x) = \frac{\pi^2}{4\cosh^2\left(\frac{\pi}{2b}x\right)} \cdot (P_s)_{circle}$$

$(P_s)_{circle}$: Surface power density of a circular chamber of radius b

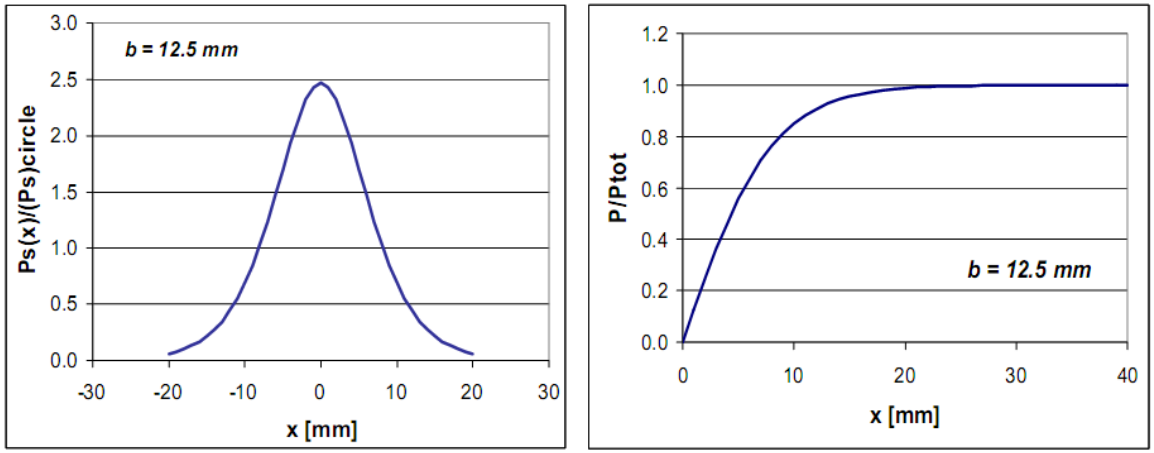

Local surface power density (left) and its integral as a function of the horizontal position x (right)

Derived $P_s(x)$ was used to compute the temperature distribution of the ceramic chambers with a 3D code, by simulating the actual air cooled structure

⇨ With 0.5 μm thick coating, the hottest point ~90° C at 500 mA,
While it rises up to ~195° C for 0.2 μm thickness (not acceptable)

6. Beam-ion instability at 500 mA

◊ Early observations

cf) R. Nagaoka et al., "Fast beam-ion …", IPAC 2010, Kyoto
R. Nagaoka et al., "Study of ion-induced…", IPAC 2011, San Sebastian

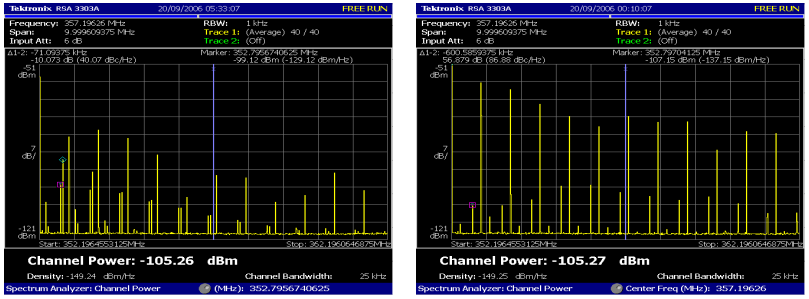

Unstable beam spectra observed in ¾ filling.
Left: "Resistive-wall dominated".
Right: Ions-dominated

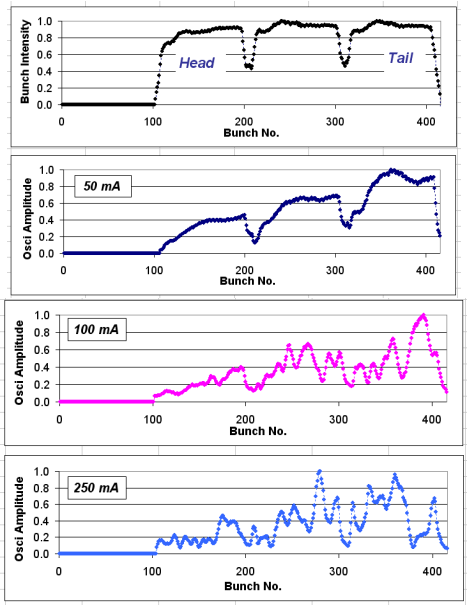

Measured vertical instability in 3/4th filling.
Top: Current distribution along a bunch train. Lower three: Oscillation amplitude at 50, 100 and 250 mA.

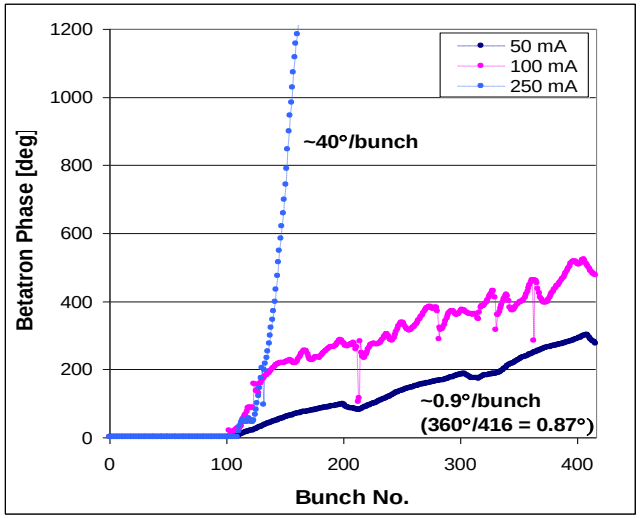

Phase of vertical bunch oscillations measured at 50, 100 and 250 mA in 3/4th filling.

◊ Way to pushing the beam current up to 500 mA

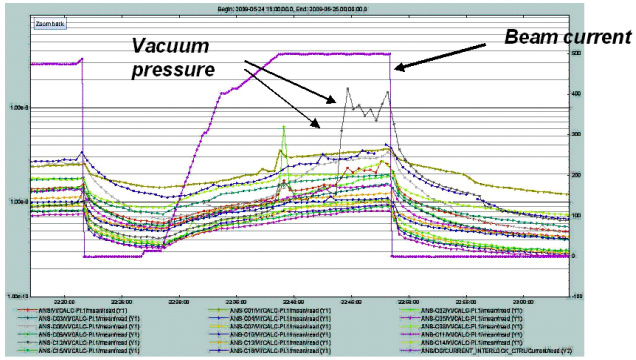

Local vacuum pressure rise followed by a beam loss encountered at 500 mA.

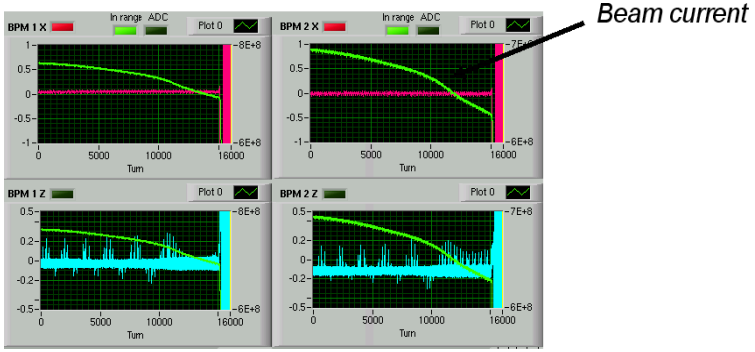

Post-mortem BPM showing a continuous beam current drop

	Filling modes	Uniform	13*(25 bunches+7 empty)	3/4th	8*(32 bunches+21 empty)
Number of bunches	nb	416	325	312	256
Number of empty buckets	h - nb	0	91	104	160
Bunch current [mA]	ib	1.20	1.54	1.60	1.95
Beam induced power	nb*(ib)^2	**601.0**	769.2	801.3	**976.6**
(tau-1)FBII	(nb)^2*(ib)^1.5	**2.28E+05**	2.02E+05	1.97E+05	**1.79E+05**

Comparison of beam-induced power and the FBII growth rate in several exotic filling patterns

Beam induced power $\propto n_b \cdot (i_b)^2$

FBII growth rate $\propto (n_b)^2 \cdot (i_b)^{1.5}$

n_b : Number of bunches

i_b : Bunch current

⇨ Reducing the beam induced heating turned out more effective than suppressing the cascading ion production with beam gaps in fighting against the FBIIs

◊ Recent analysis

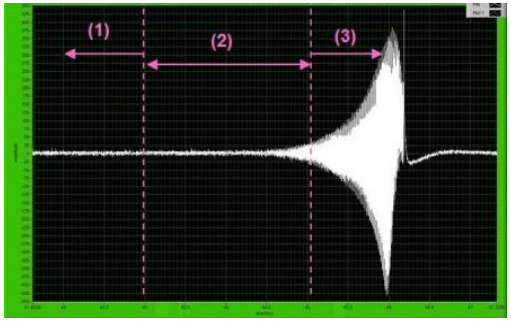

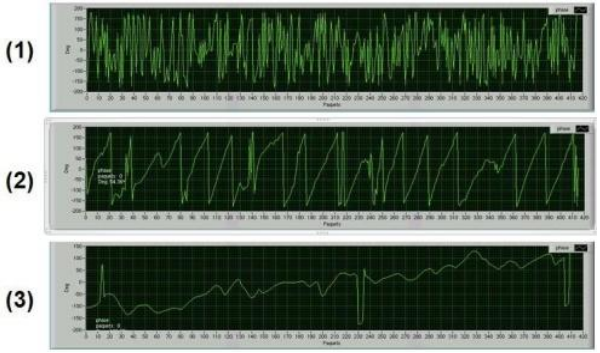

Upper: Blow up of the vertical oscillation leading to a beam loss. Lower: Betatron phase advance along a bunch train extracted at different regimes 1, 2 and 3. Measured at 500 mA with V_{RF} = 4.2 MV and ξ_V = 0

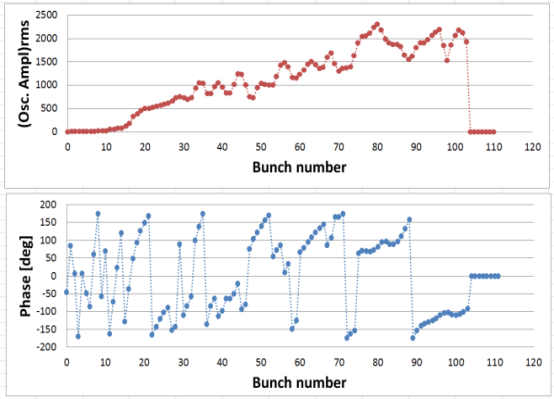

Bunch CM betatron oscillation amplitude averaged over time (upper) and oscillation phase (lower), across a bunch train obtained in the weak-weak model

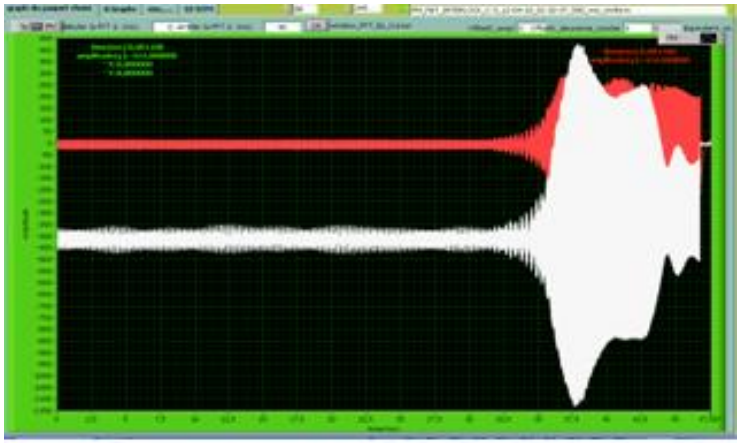

Post-mortem FBT data at 500 mA in hybrid filling mode. Red: Feedback kick. White: Beam

⇨ The action of transverse feedback against ion bursts in the presence of resistive-wall instability is being studied

7. Summary

- Beam-induced heating of the machine may well impose more stringent requirements on the vacuum chamber structures than those for beam instabilities
- Numerical simulation of wake fields turned out to be effective and useful in optimising the vacuum chamber structures
- Experiences with machine operation indicate importance of evaluating the sensitivity of deformed vacuum structures to heating
- The fast beam-ion instability encountered at 500 mA at SOLEIL is considered to originate in the beam-induced vacuum components heating

Acknowledgement

RN thanks all those colleagues of the SOLEIL accelerator team who contributed to the works presented

ANNEX

GdfidL version: mpich2-gd1-2012-12-03

Standard parameters in the wake potential calculations : Bunch length = 6 mm,

STPSZE $\geq$ 0.1 mm, *shigh* (integration length) $\geq$ 1 m

Treated frequency range $f \leq$ 30 GHz

Cluster used:

1 interactive node with 16 Intel® Xeon Dunnington hexa-core processors and 512 GB of memory (total 96 cores)

1 interactive node with 8 Intel® Xeon E7-8850 deca-core processors and 4 TB of memory (total 80 cores)

112 batch nodes with each 2 Intel® Nehalem Gainestown quad-core processors and 36 GB of memory (total 896 cores/4 TB)

And a high speed Lustre file system with 60 TB